Nature Communications

https://doi.org/10.1038/s41467-026-73158-1

Article in Press

Climate heterogeneity enhances macroclimate data-driven vegetation modeling on the Qinghai-Tibet Plateau

Received: 14 July 2025

Accepted: 3 May 2026

Cite this article as: Guan, Y., Wu, W., He, M. *et al.* Climate heterogeneity enhances macroclimate data-driven vegetation modeling on the Qinghai-Tibet Plateau. *Nat Commun* (2026). https://doi.org/10.1038/s41467-026-73158-1

Yanlong Guan, Wenqing Wu, Mengxi He, Huaikai Weng, Delong Li, Xiaoxun Huang, Deliang Chen, Shungui Zhou & Eduardo Eiji Maeda

Climate heterogeneity enhances macroclimate data-driven vegetation modeling on the Qinghai-Tibet Plateau

Yanlong Guan[1†], Wenqing Wu[1,2†], Mengxi He[1], Huaikai Weng[1], Delong Li[3], Xiaoxun Huang[1], Deliang Chen[4*], Shungui Zhou[1*], Eduardo Eiji Maeda[5,6]

[1]Fujian Provincial Key Laboratory of Soil Environmental Health and Regulation, College of Resources and Environment, Fujian Agriculture and Forestry University, Fujian 350002, China

[2] College of Ecology and Resources Engineering, Wuyi University, Wuyishan 354300, China

[3]Institute of Geographic Science and Natural Resources Research, Chinese Academy of Science, Beijing 100101, China

[4]Department of Earth System Science, Tsinghua University, Beijing 100084, China

[5]Department of Geosciences and Geography, University of Helsinki, Helsinki, Finland

[6]Finnish Meteorological Institute, Helsinki, Finland

Corresponding Author (*):

D. C (deliangchen@tsinghua.edu.cn)

S. Z (sgzhou@fafu.edu.cn)

These authors contributed equally: Yanlong Guan, Wenqing Wu.

Abstract

Climate change is altering vegetation patterns on the Qinghai-Tibet Plateau, where diverse Köppen climate zones reveal complex ecological responses. Here, we advance from a categorical view of climate, represented by Köppen-Geiger classifications, to a continuous characterization of climate heterogeneity index to better capture the link between climate and vegetation across 1- and 10-km scales. We show that climate heterogeneity strengthens vegetation–climate relationships across spatial scales, with its influence increasing 1.2-fold at coarse resolution compared to fine scales. This enhancement stems from this index providing critical heterogeneity information absent in coarse macroclimate data, thereby refining suitability predictions in regions where fine-scale topographic variability is unresolved. At finer 1-km scales, topographic heterogeneity inherently dominates, reducing the relative impact of climate heterogeneity. Overall, incorporating climate heterogeneity compensates for coarse-scale data limitations, enhancing suitability predictions where topographic detail is lost, thereby bridging macroclimate biases and microscale dynamics, and advancing robust ecological forecasting.

Introduction

Climate change is profoundly altering global ecosystems, driving shifts in vegetation communities and posing challenges for biodiversity conservation [1–3]. Accurate predictions of these ecological responses are critical for informed management and policy-making, with species distribution models (SDMs) widely used to forecast potential species ranges and community dynamics [4–6]. Yet while SDMs have become indispensable tools for ecological forecasting, their reliance on macroclimate data presents a critical limitation: they often ignore the complex, fine-scale climatic realities that shape actual vegetation distributions. This mismatch between modeling inputs and ecological reality becomes particularly problematic in heterogeneous regions, where microclimates can profoundly alter species persistence and community dynamics.

A key limitation of macroclimate-based SDMs is their oversimplification of environmental variation in heterogeneous landscapes. This can lead to overestimation of vegetation suitability or range shifts, particularly in topographically complex regions [7–10]. In such areas, microclimates—shaped by local terrain, slope, aspect, vegetation cover, and surface roughness—create diverse niches that buffer species from regional climate extremes and influence community-level responses to global change. Incorporating climate heterogeneity, encompassing both macroclimatic gradients and microclimatic variability, is therefore essential for improving ecological models. For instance, Suggitt et al., (2018) [11] showed that topographically driven microclimatic variation reduces extirpation risks for threatened species in England, while Maclean & Early, (2023) [10] found that macroclimate-based models can overestimate range shifts by more than an order of magnitude compared to those informed by microclimates. Such findings underscore that neglecting fine-scale climate variation may lead to inaccurate risk assessments and inefficient conservation planning.

Importantly, the ecological relevance of climatic data is inherently scale-dependent [12–14]. While coarse-resolution variables often obscure local environmental variation, fine-resolution models better capture microclimatic detail but face challenges such as data scarcity, increased noise, and computational demands [9,15]. This trade-off between spatial resolution and ecological fidelity represents a persistent tension in species distribution modeling. Yet, despite growing recognition of climate heterogeneity, its interaction with spatial scale remains underexplored—especially in large, topographically complex systems. For instance, coarse-scale SDMs (e.g., 10 km) tend to smooth over crucial variability, misrepresenting species–climate relationships, whereas fine-scale models (e.g., 1 km) improve spatial realism but may amplify uncertainty. Clarifying how spatial heterogeneity in climate affects model outputs across scales is thus essential for enhancing both predictive accuracy and ecological validity.

This challenge is particularly relevant to the Qinghai–Tibet Plateau—the world's largest and highest plateau—where steep environmental gradients and complex topography generate highly

heterogeneous microclimates. The region supports a rich diversity of vegetation types and ecological zones shaped by both regional climate and fine-scale topography [16,17]. In addition, decades of human activities—such as grazing, shrub encroachment, and restoration projects—have further modified vegetation composition and spatial heterogeneity. In such a dynamic and fragile ecosystem, modeling vegetation suitability requires explicit consideration of multi-scale climatic drivers. Yet, the influence of climate heterogeneity on potential vegetation distribution across spatial scales remains poorly understood—an important knowledge gap in topographically complex regions. As a natural laboratory with extreme gradients and diverse ecosystems, the Qinghai–Tibet Plateau offers the opportunity to disentangle how topographic and climatic heterogeneity modulate vegetation–climate relationships across scales.

Here, we propose a modeling framework that incorporates spatial climate heterogeneity into species distribution modeling. Our study addresses three key research questions: (1) Does climate heterogeneity improve the correspondence between predicted vegetation suitability and observed Vegetation Community Complexity (VCC) across 1-km and 10-km resolutions? (2) How does the effect of climate heterogeneity on suitability vary across scales and vegetation types? (3) How do topography and climate jointly influence the effects of spatial heterogeneity across scales? We hypothesize that incorporating spatial climate heterogeneity metrics—quantified using a Shannon entropy–based Climate Heterogeneity Index (CHI)—enhances vegetation–climate correspondence at coarser scales by compensating for macroclimate biases, with effects primarily mediated through climatic factors. Consistent with this hypothesis, incorporating climate heterogeneity into the species distribution model improves multi-scale vegetation predictions, resulting in substantially stronger vegetation responses at 10 km compared with 1 km. By capturing critical heterogeneity information absent from coarse datasets, this framework refines suitability predictions in regions where topographic variability is unresolved, advancing more robust and ecologically realistic multi-scale modeling.

Results

Climate Heterogeneity Enhances Multi-Scale Vegetation Modeling

The Köppen-Geiger classification, based on temperature and precipitation thresholds, empirically maps global vegetation distributions by linking climate variability to vegetation patterns. In the Qinghai-Tibet Plateau, we observed a strong spatial correspondence between Köppen-Geiger climate classes (Figure 1a), vegetation types (Figure 1b), and their respective heterogeneity, quantified using CHI on a 50 km × 50 km grid cell (Figure 1c). Notably, the eastern Qinghai-Tibet Plateau exhibits elevated climate and vegetation diversity, driven by topographic complexity, compared to other regions, suggesting that climate heterogeneity promotes vegetation distribution and complexity.

Vegetation community complexity quantifies the diversity of species composition and spatial distribution, calculated using the Shannon's entropy based on the proportional coverage of 12 natural vegetation types within 50 km × 50 km grid cells (see Methods for details; *Supplementary* Table S1). A higher VCC indicates greater complexity of vegetation community (Figure 1d). This metric underpins our correlation analyses, with the correlation between VCC and suitability increasing from ~0.25 to ~0.28 at 1 km, and from ~0.25 to ~0.30 at 10 km when CHI is incorporated into MaxEnt models (Figure 2; *Supplementary* Figure S1). These results indicate that CHI captures essential spatial variability in climate, thereby improving the ecological realism of suitability predictions (*Supplementary* Figure S2).

CHI Enhances the Vegetation Response at Macroclimate Scales

To evaluate the impact of climate heterogeneity on vegetation distribution across scales, we developed a comparative framework analyzing MaxEnt outputs with and without CHI as a predictor. The potential change in vegetation suitability, quantified as |ΔS| (see Methods), was consistently more pronounced at 10 km resolution than at 1 km (Figure 3; *Supplementary* Figures S3–S8). Spatial patterns of |ΔS| reveal more pronounced and spatially coherent CHI-induced improvements in suitability at 10 km, particularly across the eastern Qinghai–Tibet Plateau (Figure 3a, b), where vegetation community complexity is highest.

Across vegetation types, a clear scale-dependent pattern emerged. The average correlation coefficient between grid-based VCC and CHI-driven suitability across 12 vegetation classes increased from 0.28 ± 0.24 at 1 km to 0.30 ± 0.24 at 10 km (Figure 2). Consistent with this pattern, the average |ΔS| at 10 km resolution is approximately 1.2-fold greater than at 1-km, indicating that the influence of climate heterogeneity on vegetation suitability strengthens as spatial resolution becomes coarser (*Supplementary* Figure S9). Vegetation-type analyses further show that |ΔS| at 10 km is consistently larger than at 1 km (Figure 3c).

Notably, alpine vegetation types (e.g., AM, AG, AV, AD) show relatively weaker ΔS values, reflecting their dominance in the inland Qinghai–Tibet Plateau where extreme macroclimatic conditions prevail (*Supplementary* Figure S10-S11). This pattern does not imply reduced sensitivity of alpine vegetation to microclimatic variability; rather, it reflects that under coarse-resolution climate representations, vegetation distributions in these regions are already strongly constrained by temperature and moisture extremes, likely leaving limited additional explanatory power for spatial heterogeneity. In contrast, the eastern Qinghai–Tibet Plateau, characterized by greater vegetation complexity, displays apparently higher CHI-driven |ΔS| values. These findings reinforce that regional climate heterogeneity enhances the ecological sensitivity of vegetation to climatic variability, particularly under coarser macroclimatic conditions.

CHI Compensates for Macroclimate Bias via Heterogeneity

We applied Random Forest (RF) and Partial Least Squares Structural Equation Modeling (PLS-SEM) to quantify the contributions of topographic and climatic factors to ΔS across spatial resolutions. RF analyses reveal a clear scale-dependent shift in dominant drivers (Figures 4a-4c; *Supplementary* Tables S4-S5). Specifically, regional climate apparently influences ΔS at 10-km resolution, with its relative importance increasing from 32.4% at 1-km to 34.5% at 10-km. This enhancement is spatially concentrated in the eastern Qinghai–Tibet Plateau, where vegetation complexity is highest. In contrast, topography exerts stronger control at 1-km resolution (27.4%), but its importance decreases slightly at 10-km (26.3%; Figure 4d–f), reflecting a scale-dependent shift in dominant drivers.

To further interpret these scale-dependent relationships, we used PLS-SEM to examine latent variable pathways (Topography → ΔS, Climate → ΔS, and Topography → Climate). The model showed good fit (Figure 5a, b; *Supplementary* Figures S16-S17), with a focus on high-feature-importance areas in the eastern Plateau. At 1-km, topography has a strong direct effect on ΔS (0.553), while its indirect effect via climate is modest ($-0.061 \times 0.68 \approx -0.041$), consistent with microclimatic heterogeneity dominating fine-scale suitability. In contrast, at 10-km, topography's direct influence weakens (0.445), while its indirect effect through climate strengthens ($-0.209 \times 0.662 \approx -0.138$), accompanied by a stronger direct climatic influence (–0.209). These findings demonstrate a scale transition from topography-dominated to climate-dominated control on ΔS.

Mechanistically, this pattern indicates that as spatial resolution coarsens, fine-scale topographic detail—and its microclimatic influence—becomes smoothed, thereby amplifying CHI's compensatory role in representing environmental heterogeneity. In other words, CHI captures the missing heterogeneity in coarser climate datasets, offsetting macroclimate bias and improving suitability predictions. Together, the RF and PLS-SEM results reveal that CHI acts as a heterogeneity surrogate that bridges the information gap between microclimate-driven fine-scale variation and macroclimate-driven coarse-scale modeling.

Discussion

Our findings underscore the critical importance of incorporating spatial heterogeneity metrics into ecological modeling frameworks for conservation planning in complex mountain ecosystems. On the Qinghai–Tibet Plateau, where biotic responses are closely linked to fine-scale environmental gradients, we show that climate heterogeneity enhances the correspondence between predicted habitat suitability and observed vegetation community patterns—especially in the topographically diverse eastern region. This area features a rich mosaic of temperate and alpine vegetation formations, and the improved model performance there suggests that climate heterogeneity captures key ecological nuances that traditional climate and topographic predictors often overlook. As a result, climate heterogeneity offers a scalable and transferable metric for informing

landscape-level conservation strategies, including the identification of ecological refugia, prioritization of restoration efforts, and delineation of climate-resilient corridors.

Our results demonstrate that climate heterogeneity, quantified by CHI, enhances the reliability of vegetation distribution models by strengthening the link between environmental variability and community-level complexity. Incorporating CHI into MaxEnt increases the correlation between VCC and suitability from 0.28 ± 0.238 at 1 km to 0.30 ± 0.24 at 10 km, indicating that areas with higher climate heterogeneity support more complex vegetation communities and are better captured by the models. Additionally, CHI integration improves the detection of ecological thresholds, as reflected by a 1.2-fold increase in |ΔS| variability at 10 km relative to 1 km. These findings have practical implications for biodiversity management: regions with high CHI but low VCC may be vulnerable to degradation, whereas areas with both high CHI and high VCC (e.g., the eastern Qinghai–Tibet Plateau) could serve as biodiversity reservoirs under climate change.

Furthermore, climate heterogeneity offers a transferable tool for comparative ecological studies in other mountainous or climatically variable regions, such as the Andes or the Himalayas. By standardizing the quantification of spatial climate diversity, it supports cross-regional assessments of vegetation–climate relationships and provides a unifying metric for global mountain biodiversity research [18,19]. As climate change accelerates biome shifts and alters vegetation–climate equilibria, such standardized heterogeneity indices will become increasingly valuable for improving the transferability of ecological models while maintaining sensitivity to local context. Overall, our study presents climate heterogeneity not only as a methodological enhancement but also as a practical conservation tool with broad geographic and thematic relevance.

While integrating climate heterogeneity appears to improve model performance, our findings also highlight important limitations that point to key directions for future research. First, the contribution of climate heterogeneity to model accuracy is highly scale-dependent and biome-specific. In particular, alpine and high-cold desert vegetation types—dominant in the central and western Qinghai–Tibet Plateau—show minimal improvement with the inclusion of climate heterogeneity, with ΔS values often below 2%. This suggests that in environments shaped by strong environmental filtering—where climatic conditions are highly deterministic and ecological niches are narrow—heterogeneity metrics such as climate heterogeneity may have limited ecological relevance. In such contexts, the simplicity of vegetation structure and restricted species pools likely reduce ecosystem sensitivity to spatial climatic variation, thereby constraining the utility of diversity-based indices [9,20,21].

Second, our current approach relies on static, spatially explicit indices derived from land cover and climate classifications [22,23], limiting our ability to capture dynamic ecological processes such as succession, disturbance regimes (e.g., grazing, fire), or species migration. Additionally, climate heterogeneity is sensitive to the resolution and classification schemes of input datasets [24,25]. For

example, changes in the number or granularity of Köppen–Geiger classes directly influence calculated heterogeneity levels, potentially introducing inconsistencies when comparing across regions or time periods. Addressing this issue requires standardized protocols for calculating heterogeneity, ideally through harmonized classification systems and explicit incorporation of uncertainty.

To better understand ecological role of climate heterogeneity, future studies should incorporate high-resolution, field-validated biodiversity and trait datasets. This would allow for stronger links between climate heterogeneity and not only vegetation structure but also ecological function [26,27]. Integrating plant functional types, dispersal strategies, and phenological variability into heterogeneity-based models could refine predictions and yield insights into community assembly processes under climate stress. Furthermore, temporal extensions of climate heterogeneity—using long-term climate variability or future scenario projections—would allow the development of dynamic heterogeneity indices that reflect climate stability and variability over ecologically meaningful timescales.

Finally, moving beyond vegetation-focused approaches, applying climate heterogeneity in faunal distribution models and ecosystem service assessments could uncover new dimensions of its ecological significance. The potential to generalize climate heterogeneity–enhanced models across taxa and ecosystem functions holds promise for building integrated biodiversity monitoring systems, especially in data-scarce but ecologically critical regions like the Qinghai–Tibet Plateau. Ultimately, bridging spatial heterogeneity metrics with ecological theory, remote sensing, and field observations will be essential for developing predictive models that are both mechanistically grounded and conservation-relevant in a rapidly changing world [28–30].

Methods

Climate and environmental data

In this study, we collected average monthly temperature and precipitation data set (1991-2020) from Beck et al., (2023)[6], which were compiled from multiple observation-based and topographically corrected sources, including WorldClim v2, CHELSA v1.2/v2.1, and CHPclim. In this dataset, these climatic variables are resampled to multiple spatial resolutions using bilinear interpolation. In this study, we explored two resolutions, a fine-scale microclimate dataset of 0.008333° (~ 1 km) and a coarse macroclimate dataset of 0.1° (~10 km).

We also used the Köppen–Geiger climate classification map (1991–2020), provided by Beck et al., (2023) [6], at 1 km and 10 km resolutions. Köppen–Geiger climate classification system, is a widely adopted framework that aims to empirically map vegetation distributions around the world based on monthly air temperature and precipitation thresholds [3] (*Supplementary* Table S6). It divides global terrestrial climates into five major types—tropical, arid, temperate, cold, and polar—and

further into 30 subtypes based on the seasonal patterns and magnitude of thermal and hydrological conditions. In this study, these categorical climate types were subsequently used to compute climate heterogeneity on the Qinghai-Tibet Plateau.

Vegetation distribution data were obtained from the 30-m resolution vegetation maps of the Tibetan Plateau (2020)[32], hosted by the National Tibetan Plateau Data Center of China. These maps were generated using a random forest algorithm on Google Earth Engine, integrating terrain, climate, and multi-temporal Landsat imagery, and achieved high classification accuracy (overall accuracy = 95.00%, Kappa = 0.95). The dataset provides a reliable, high-resolution basis for vegetation modeling on the plateau. Vegetation was classified into 16 types; only codes 1–12, representing natural vegetation, were used in this study (*Supplementary* Table S1). Non-vegetated categories, such as lakes and wetlands (codes 13–16), were excluded.

To examine the effects of spatial resolution on vegetation distribution patterns across the Tibetan Plateau, we employed 18 environmental variables at two spatial scales (1 km and 10 km). These include 9 generalized Köppen climate variables, 4 bioclimatic variables, 4 topographic variables, and 1 soil moisture variable (*Supplementary* Table S7). All variables except the Köppen indices were originally at 1 km resolution and resampled to 10 km using bilinear interpolation to ensure consistency. To mitigate multicollinearity, we performed variable selection and ultimately retained 8 variables as input for the MaxEnt model.

Climate Heterogeneity

To capture climate spatial heterogeneity, we calculated the a Climate Heterogeneity Index (CHI), derived from Shannon's entropy[28], using 1-km Köppen–Geiger climate maps[31] aggregated within 50 × 50 km grid cells, thereby quantifying regional-scale heterogeneity while retaining local variation. CHI is computed as,

$$\mathrm{CHI} = \sum_{i=1}^{S} p_i \ln p_i \tag{1}$$

where S represents the total number of climate types within a grid cell, and p_i denotes the proportion of area covered by climate type i. Compared with categorical climate/vegetation classes, CHI provides a continuous and scale-robust measure of heterogeneity, reducing boundary effects and improving validation performance (*Supplementary* Figures S18-S21).

Vegetation community Complexity

Vegetation community complexity (VCC) was quantified following Su *et al*., (2022) [33], and aggregated to 50 km × 50 km grid cells. VCC characterizes the structural complexity of vegetation communities and was derived from Shannon's entropy using the proportional coverage of 12 natural vegetation types across the Plateau. This grid-based VCC metric supports multi-scale ecological modeling and reflects the spatial and compositional diversity of natural vegetation communities. For each 50 km × 50 km grid cell, we calculated the proportional coverage (p_i) of each vegetation type and derived the Shannon's entropy as,

$$\mathrm{VCC} = \sum_{i=1}^{12} p_i \ln p_i \tag{2}$$

where higher VCC values indicate greater vegetation structural heterogeneity and compositional diversity. The 50 km resolution was chosen to balance spatial heterogeneity representation with computational feasibility, ensuring sufficient sampling of vegetation mosaics across the complex terrain of the Qinghai–Tibet Plateau (*Supplementary* Figure S22).

Suitability (S) Modeling and ΔS calculation

We employed MaxEnt v3.4.3, implemented via ENMTools 1.0.4, to model the suitability distribution of 12 vegetation types on the Tibetan Plateau. Models were calibrated with 10,000 background points randomly sampled across the study area. Linear, quadratic, and product features were used to balance predictive power with interpretability. The regularization multiplier was set to the default value of 1, providing adequate control of model complexity under moderate feature settings. Maximum iterations were set to 5,000 with a convergence threshold of 10^{-5}. Replication was performed with 10-fold cross-validation, and 25% of occurrence records were randomly withheld for testing. Logistic output was used to estimate habitat suitability. These settings follow the reproducibility checklist proposed by Feng et al. (2019) [38] and Zurell et al. (2020) [39], ensuring transparency and comparability with other ecological niche modeling studies (see Supplementary Note 1 for details).

A total of 18 candidate environmental variables were initially compiled, covering climatic, topographic, and edaphic dimensions (*Supplementary* Table S7). To mitigate multicollinearity, pairwise Pearson's correlation coefficients were calculated and only those variables with $|r| < 0.8$ were retained. Finally, 8 variables were selected as input for the Maxtent model: Elevation, Roughness, Temperature in the coldest month (Tcold), Accumulated temperature or growing degree days of daily temperature >5°C (GDD5), Soil moisture (SM), Precipitation in the driest month in winter (Pwdry), Precipitation in the wettest month in summer (Pswet), and Precipitation in the driest month in summer (Psdry).

Suitability (S) outputs were trained using 10-fold cross-validation with 10 replicates per vegetation type. Habitat suitability maps were generated for each replicate, and final maps were obtained via AUC-weighted averaging. AUC values above 0.8 were used to assess predictive performance. Four scenarios were tested: 1-km with/without CHI and 10-km with/without CHI. CHI's impact was quantified as:

$$|\Delta S| = |S_{with\_CHI} - S_{without\_CHI}| \quad (3)$$

where |ΔS| measures the magnitude of CHI-induced variability at the grid-cell level.

Factors influencing ΔS variability across scales

To quantitatively assess the climatic and topographic influences on the ΔS across different resolutions, we employed Random Forest (RF) method to model ΔS for 12 vegetation types [35]. The model incorporated 12 predictors, including 8 key variables selected via Maxent modeling and 4 representative climatic and topographic variables (*Supplementary* Table S8). All models passed the significance test, with r^2 around 0.61. We then extracted the decision paths of all trees and quantified the contribution of each feature to every sample's trajectory, allowing for individual-level feature importance scoring and identification of the dominant environmental drivers of ΔS. This enabled a fine-scale mapping of the spatial influence strength of each predictor within a 50 km × 50 km grid framework. Subsequently, for each vegetation type, we averaged the individual-level importance values of the climatic and topographic variables, yielding climate and topography impact scores.

To further explore the structural mechanisms by which topographic and climatic factors influence the spatial heterogeneity of ΔS, we employed Partial Least Squares Structural Equation Modeling (PLS-SEM) to assess the direct and indirect effects of environmental variables on ΔS [36,37]. As a causal modeling approach well-suited for multivariate, high-dimensional, and non-normally distributed data, PLS-SEM enables the effective identification of path structures among latent variables and the quantification of their relative contributions. In this study, we assumed that topographic factors exert both direct effects on suitability and indirect effects via modulation of climatic conditions, thus forming a hierarchical path structure. In constructing the model, three latent variables were defined to represent different ecological factor hierarchies: 1) Topography: including Elevation, Roughness, and Slope; 2) Climate: including Tcold, Pwdry, Pswet, and Psdry; and 3) ΔS: suitability response was consists of 12 vegetation types.

Data Availability

The average monthly temperature and precipitation datasets (1991–2020) and the derived Köppen–Geiger climate classification map are publicly available from www.gloh2o.org/koppen. The 30 m vegetation maps of the Qinghai–Tibet Plateau (1990–2020) are available from the National Tibetan Plateau Data Center at https://data.tpdc.ac.cn/en/data/0c84a954-435d-45f4-bf42-d561f7c7da2a. Soil moisture data were obtained from https://data.tpdc.ac.cn/zh-hans/data/b611fb43-c18c-4966-a85c-949ce1ca60f2, and fractional vegetation cover (FVC) data were obtained from http://www.glass.umd.edu/FVC/AVHRR/. Topographic variables were obtained from http://www.earthenv.org/topography. Bioclimatic variables were obtained from https://www.sciengine.com/CSD/doi/10.11922/11-6035.csd.2022.0003.zh. All processed data generated in this study, including the Climate Heterogeneity Index (CHI), vegetation community complexity (VCC), suitability metrics, and derived modelling outputs, are publicly available via Figshare under accession code https://doi.org/10.6084/m9.figshare.30327469. Source data are provided with this paper.

Code Availability

Our code is available at https://github.com/xioaguan/ClimateHeterogeneity [40].

References

1. García, R., Cabeza, M., Rahbek, C. & Araújo, M. B. Multiple dimensions of climate change and their implications for biodiversity. *Science* **344**, 1247579 (2014).
2. Pecl, G. T. et al. Biodiversity redistribution under climate change: impacts on ecosystems and human well-being. *Science* **355**, eaai9214 (2017).
3. Chen, D. et al. Framing, context, and methods. In Climate Change 2021: The Physical Science Basis. Contribution of Working Group I to the Sixth Assessment Report of the Intergovernmental Panel on Climate Change (eds Masson-Delmotte, V. et al.) Ch. 1, 105–304 (Cambridge Univ. Press, 2021).
4. Zu, K. et al. Elevational shift in seed plant distributions in China's mountains over the last 70 years. *Glob. Ecol. Biogeogr*. **32**, 1098–1112 (2023).
5. Petitpierre, B. et al. Will climate change increase the risk of plant invasions into mountains? *Ecol. Appl.* **26**, 530–544 (2016).
6. Beck, H. E. et al. Present and future Köppen-Geiger climate classification maps at 1-km resolution. *Sci. Data* **5**, 180214 (2018).
7. De Frenne, P. et al. Global buffering of temperatures under forest canopies. *Nat. Ecol. Evol*. **3**, 744–749 (2019).

8. Kemppinen, J. et al. Microclimate, an important part of ecology and biogeography. *Glob. Ecol. Biogeogr*. **33**, 1149–1163 (2024).

9. Ismaeel, A. et al. Patterns of tropical forest understory temperatures. *Nat. Commun*. **15**, 579 (2024).

10. Maclean, I. M. D. & Early, R. Macroclimate data overestimate range shifts of plants in response to climate change. *Nat. Clim. Chang*. **13**, 484–490 (2023).

11. Suggitt, A. J. et al. Extinction risk from climate change is reduced by microclimatic buffering. *Nat. Clim. Chang*. **8**, 713–717 (2018).

12. Kemppinen, J., Niittynen, P., Riihimäki, H. & Luoto, M. Modelling soil moisture in a high-latitude landscape using LiDAR and soil data. Earth Surf. Process. *Landf*. **43**, 1019–1031 (2018).

13. Piao, S. et al. Characteristics, drivers and feedbacks of global greening. *Nat. Rev. Earth Environ*. **1**, 14–27 (2020).

14. Cui, D., Liang, S., Wang, D. & Liu, Z. A 1-km global dataset of historical (1979–2013) and future (2020–2099) Köppen-Geiger climate classification and bioclimatic variables. *Earth Syst. Sci. Data* **13**, 5087–5107 (2021).

15. Lembrechts, J. J. et al. SoilTemp: a global database of near-surface temperature. *Glob. Chang. Biol*. **26**, 6616–6629 (2020).

16. Yao, T. et al. The imbalance of the Asian water tower. *Nat. Rev. Earth Environ*. **3**, 618–632 (2022).

17. Ehlers, T. A. et al. Past, present, and future geo-biosphere interactions on the Tibetan Plateau and implications for permafrost. *Earth-Sci. Rev*. **234**, 104197 (2022).

18. Holzmann, K. L., Walls, R. L. & Wiens, J. J. Accelerating local extinction associated with very recent climate change. *Ecol. Lett*. **26**, 1877–1886 (2023).

19. Rahbek, C. et al. Humboldt's enigma: what causes global patterns of mountain biodiversity? *Science* **365**, 1108–1113 (2019).

20. Wang, J. et al. Temperature changes induced by biogeochemical and biophysical effects of bioenergy crop cultivation. *Environ. Sci. Technol*. **57**, 2474–2483 (2023).

21. Li, D., Wu, S., Liu, L., Zhang, Y. & Li, S. Vulnerability of the global terrestrial ecosystems to climate change. *Glob. Chang. Biol*. **24**, 4095–4106 (2018).

22. Peel, M. C., Finlayson, B. L. & McMahon, T. A. Updated world map of the Köppen-Geiger climate classification. *Hydrol. Earth Syst. Sci*. **11**, 1633–1644 (2007).

23. Chen, D. & Chen, H. W. Using the Köppen classification to quantify climate variation and change: an example for 1901–2010. *Environ. Dev*. **6**, 69–79 (2013).

24. Guan, Y. et al. From a spatial structure perspective: spatial-temporal variation of climate redistribution of China based on the Köppen–Geiger classification. *Geophys. Res. Lett*. **49**, e2022GL099319 (2022).

25. Guan, Y. et al. Intensified fragmentation and shrinkage of the polar climate zone in the Arctic. *Int. J. Climatol*. **41**, 4573–4586 (2021).

26. Lang, W. et al. Phenological divergence between plants and animals under climate change. *Nat. Ecol. Evol.* **8**, 1899–1911 (2024).

27. Yue, C. et al. Contributions of ecological restoration policies to China's land carbon balance. *Nat. Commun*. **15**, 9708 (2024).

28. Guan, Y. et al. Elevation regulates the response of climate heterogeneity to climate change. *Geophys. Res. Lett*. **51**, e2024GL109483 (2024).

29. Coelho, M. T. P. et al. The geography of climate and the global patterns of species diversity. *Nature* **622**, 537–544 (2023).

30. Stein, A., Gerstner, K. & Kreft, H. Environmental heterogeneity as a universal driver of species richness across taxa, biomes and spatial scales. *Ecol. Lett*. **17**, 866–880 (2014).

31. Beck, H. E. et al. High-resolution (1 km) Köppen-Geiger maps for 1901–2099 based on constrained CMIP6 projections. *Sci. Data* **10**, 724 (2023).

32. Wu, F., Ren, H. & Zhou, G. The 30 m vegetation maps from 1990 to 2020 in the Tibetan Plateau. *Sci. Data* **11**, 802 (2024).

33. Su, Y. et al. Human-climate coupled changes in vegetation community complexity of China since 1980s. *Earths Future* **10**, e2021EF002553 (2022).

34. Phillips, S. J., Anderson, R. P. & Schapire, R. E. Maximum entropy modeling of species geographic distributions. *Ecol. Model*. **190**, 231–259 (2006).

35. Biau, G. Analysis of a random forests model. *J. Mach. Learn. Res*. **13**, 1063–1095 (2012).

36. Tallavaara, M., Eronen, J. T. & Luoto, M. Productivity, biodiversity, and pathogens influence the global hunter-gatherer population density. *Proc. Natl Acad. Sci. USA* **115**, 1247–1252 (2018).

37. Bai, Y., & Tang, Z. Enhanced effects of species richness on resistance and resilience of global tree growth to prolonged drought. *Proc. Natl Acad. Sci. USA* **121**, e2410467121 (2024).

38. Feng, X., Park, D. S., Liang, Y. et al. A checklist for maximizing reproducibility of ecological niche models. *Nat. Ecol. Evol*. **3**, 1382–1395 (2019).

39. Zurell, D., Franklin, J., König, C. et al. A standard protocol for reporting species distribution models. *Ecography* **43**, 1261–1277 (2020).

40. Guan Y. ClimateHeterogeneity (v1.0): Climate heterogeneity enhances macroclimate data-driven vegetation modeling on the Qinghai-Tibet Plateau. Zenodo, https://doi.org/10.5281/zenodo.18295341, (2026).

Acknowledgments

We thank the data providers and developers of the publicly available datasets used in this study, including the Köppen–Geiger climate classification, vegetation, soil moisture, fractional vegetation cover, topographic, and bioclimatic datasets. We are grateful to colleagues and collaborators for helpful discussions and constructive feedback that improved this work. We also thank the reviewers for their constructive comments, which helped improve the clarity and rigor of this work.

Funding

This study was supported by the National Natural Science Foundation of China (42525702, **S.Z.**; 42477508, **Y.G.**; W2521031, **Y.G.**; and 42407630, **X.H**.), Natural Science Foundation of Fujian Province (2024J01132005; **Y.G**.), and the Open Fund of Fujian Provincial Key Laboratory of Eco-Industrial Green Technology（WYKF-EIGT2024-1, **Y.G**.). **D.C.** was supported by Tsinghua University (100008001). **E.E.M.** is funded by the Research Council of Finland (363501).

Author Contributions Statement

Y.G. designed the study. W.W. and Y.G. performed the analysis and wrote the manuscript. H.W., D.L. and M.H. performed the species distribution model experiments. W.W., Y.G and X.H coordinated the revision and language editing. D.C., S.Z. and E.E.M. performed the formal analysis and supervised the revision. All authors discussed the results and reviewed the manuscript.

Competing Interests Statement

The authors declare no competing interests.

Figure legends

Figure 1. Maps of climate and vegetation. a,**c**, Spatial distributions of Köppen-Geiger climate classes (**a**) and its heterogeneity (**c**) quantified by Shannon's entropy at a fixed 50 km × 50 km grid cell, highlighting regional climate gradients and diversity. **b**,**d**, Spatial distributions of vegetation types (**b**) and their complexity (**d**) quantified using the same entropy metric, indicating spatial patterns of ecological diversity and their correspondence with climate heterogeneity.

Figure 2. Correlations between vegetation community complexity (VCC) and Suitability across vegetation types. Cyan and red represent the analyses at 1-km and 10-km resolutions, respectively. Bars indicate correlations for individual vegetation types, while boxplots summarize the overall correlations modelled with CHI. Pearson correlations were calculated across 1145 independent spatial units (50 km × 50 km grid cells). In box plots, the center line indicates the median; the box bounds represent the interquartile range (25th–75th percentiles); whiskers extend to 1.5 × the interquartile range. Statistical significance of Pearson correlations was assessed using two-sided tests (degrees of freedom, 1143). Exact *r* values and corresponding *P* values for each vegetation type are provided in Supplementary Table S2. *** indicates $P < 0.001$. Incorporating climate heterogeneity (CHI) into MaxEnt models consistently increases this correlation, indicating improved ecological realism of suitability predictions. The stronger effect at 10 km resolution highlights the role of CHI in compensating for coarse-resolution macroclimate biases. Correlations are generally positive across vegetation types, except for alpine vegetation classes (e.g. AM, AG, AV, AD) where extreme climatic constraints reduce vegetation–climate correspondence. Abbreviations: evergreen broad-leaved forest (EBF), evergreen coniferous forest (ECF), coniferous and broad-leaved mixed forest (CBF), deciduous broad-leaved forest (DBF), deciduous coniferous forest (DCF), scrub (SCR), alpine scrub meadow (ASM), alpine meadow (AM), alpine grassland (AG), alpine vegetation (AV), alpine desert (AD), and cultivated vegetation (CV). Source data are provided as a Source Data file.

Figure 3. Comparisons of |ΔS| at 1 km and 10 km resolutions. a,**b**, Spatial distributions of |ΔS| at 1-km (**a**) and 10-km (**b**) resolutions. **c,** Distributions of |ΔS| at 1-km and 10-km resolutions, derived from the average Maxent model outputs for 12 vegetation classes. All model outputs exhibit robust performance (AUC > 0.8; *Supplementary* Figure S12-S15). Each |ΔS| value represents the absolute difference in predicted suitability for an independent spatial unit (50 km × 50 km grid cell) between models excluding and including CHI. $n = 1145$ denotes the number of independent grid cells used in each resolution-specific comparison. In violin plots, the width represents the kernel probability density of |ΔS| values. The central white dot indicates the median, and the thick black bar denotes the interquartile range (25th–75th percentiles). Differences

between resolutions were assessed using two-sided *t*-tests. Exact *P* values are reported in Supplementary Table S3, and *** indicates $P < 0.001$. Across vegetation types, the CHI effect is consistently stronger at 10 km, underscoring its compensatory role under coarse climate data. Source data are provided as a Source Data file.

Figure 4. Impacts of topography and climate on ΔS at 1 km and 10 km resolutions. a,b, Distributions of climatic feature importance, calculated as the sum of climatic variables for each independent 50 km × 50 km grid cell (n = 1145), including Temperature in the coldest month (Tcold), Precipitation in the driest month in winter (Pwdry), Precipitation in the wettest month in summer (Pswet), and Precipitation in the driest month in summer (Psdry). **c**, Distributions of climatic feature importance summarized across 12 vegetation types ($n = 12$); these summaries are descriptive and do not involve statistical significance testing. **d,e,** Distributions of topographical feature importance, calculated as the sum of topographical variables for each independent grid cell ($n = 1145$), including Elevation, Slope, and Roughness. **f**, Distributions of topographical feature importance summarized across 12 vegetation types ($n = 12$); these summaries are descriptive. In all box plots, the center line indicates the median; the box bounds represent the interquartile range (25th–75th percentiles); whiskers extend to 1.5 × the interquartile range. Comparisons between resolutions highlight a scale-dependent shift from topography-dominated control at fine resolution toward climate-dominated control at coarser resolution. Source data are provided as a Source Data file.

Figure 5. The direct and indirect effects of topography and climate variables on ΔS. Structural equation models illustrating the pathways linking topography, climate, and ΔS at (**a**) 1 km and (**b**) 10 km spatial resolutions. All path coefficients are standardized. Statistical significance was assessed using two-sided bootstrap tests (**$P < 0.01$). The model was fitted using independent 50 km × 50 km grid cells ($n = 1145$). Full latent variable paths (e.g., Topography → Climate, Topography → ΔS, Climate → ΔS) and significance ($p < 0.01$) are reported in the text; additional details in *Supplementary* Figure S16-S17. Source data are provided as a Source Data file.

Editorial Summary:
Climate heterogeneity strongly shapes how vegetation responds to environmental change, but is often overlooked in large-scale modelling. This study shows that incorporating climate heterogeneity improves vegetation suitability predictions, especially at coarse spatial resolutions.
Peer review information: *Nature Communications* thanks the anonymous reviewer(s) for their contribution to the peer review of this work. A peer review file is available.

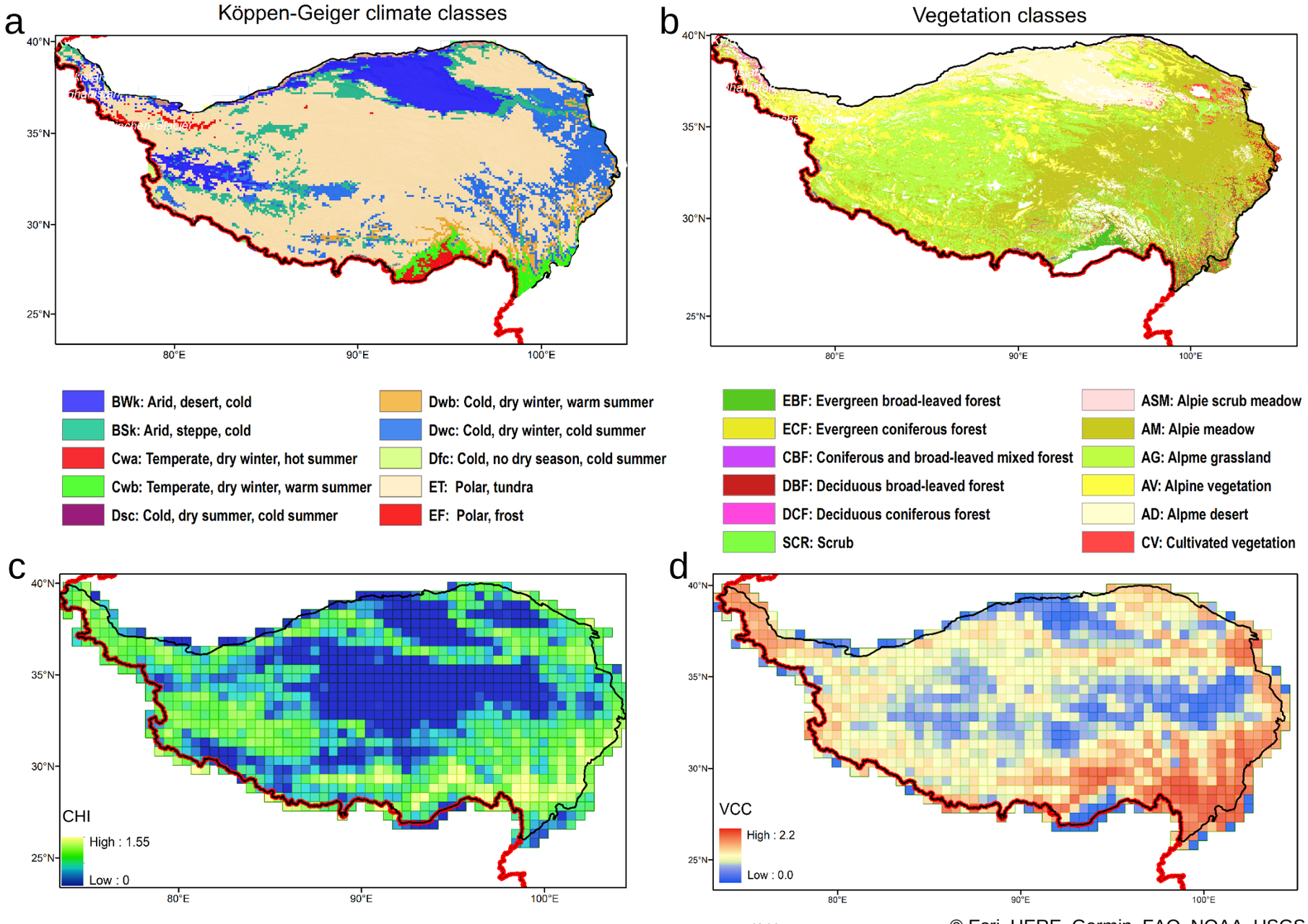

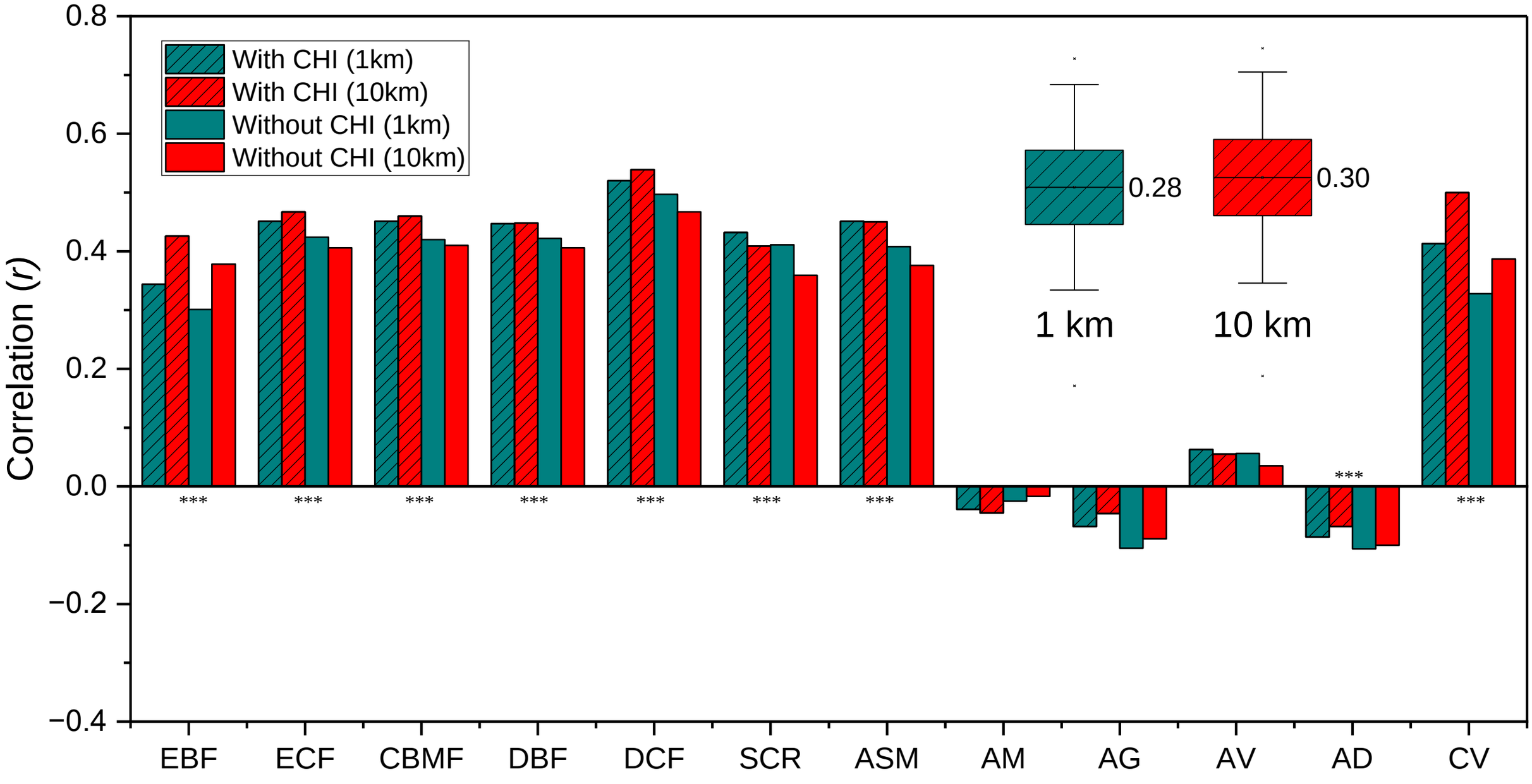
With CHI (1km)
With CHI (10km)
Without CHI (1km)
Without CHI (10km)
Correlation (r)
0.8
0.6
0.4
0.2
0.0
−0.2
−0.4
0.28
0.30
1 km
10 km
***
EBF
ECF
CBMF
DBF
DCF
SCR
ASM
AM
AG
AV
AD
CV

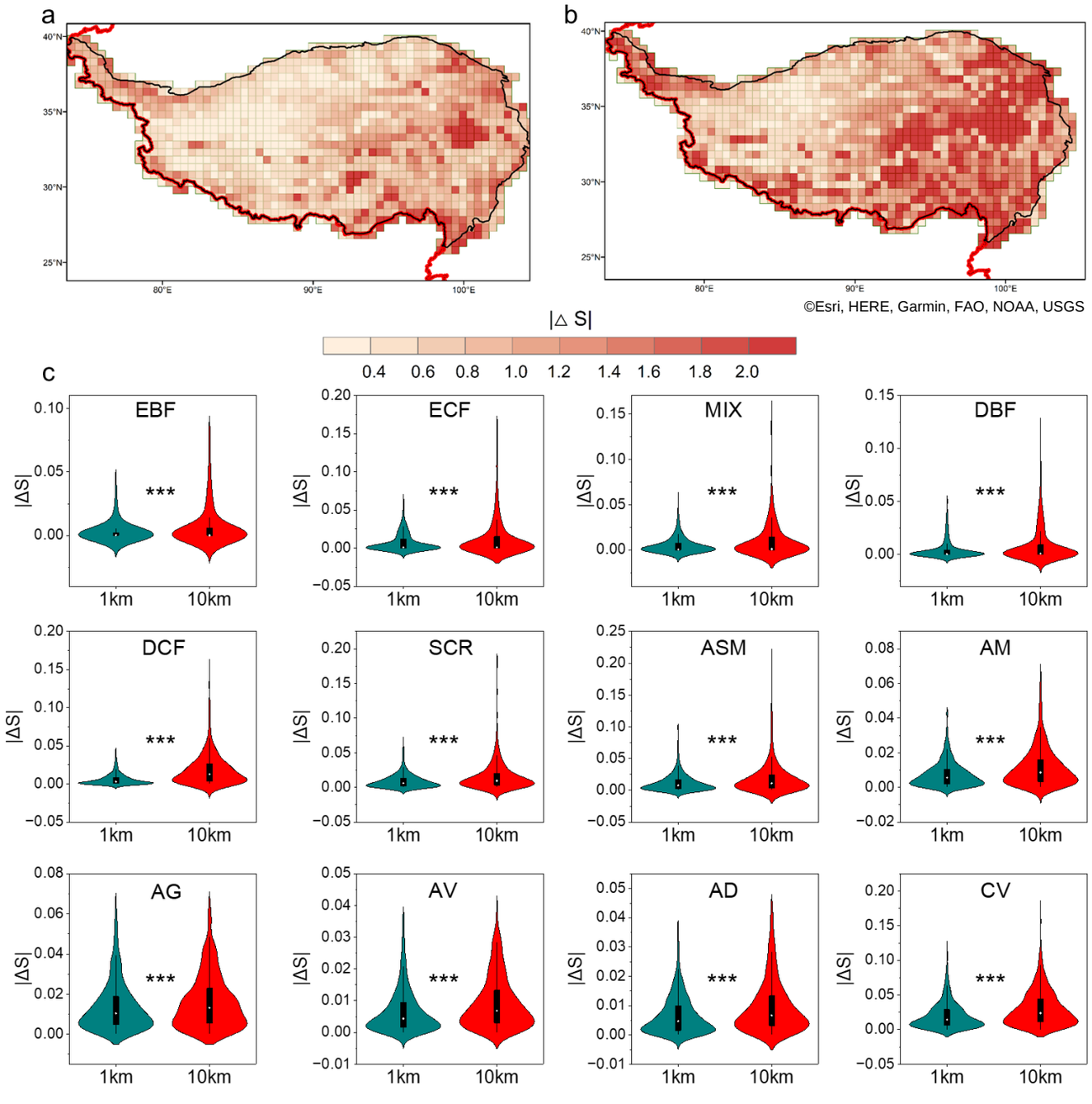
a
b
40°N
35°N
30°N
25°N
80°E
90°E
100°E
©Esri, HERE, Garmin, FAO, NOAA, USGS
|△ S|
0.4 0.6 0.8 1.0 1.2 1.4 1.6 1.8 2.0
c
EBF
ECF
MIX
DBF
DCF
SCR
ASM
AM
AG
AV
AD
CV
|ΔS|
***
1km
10km

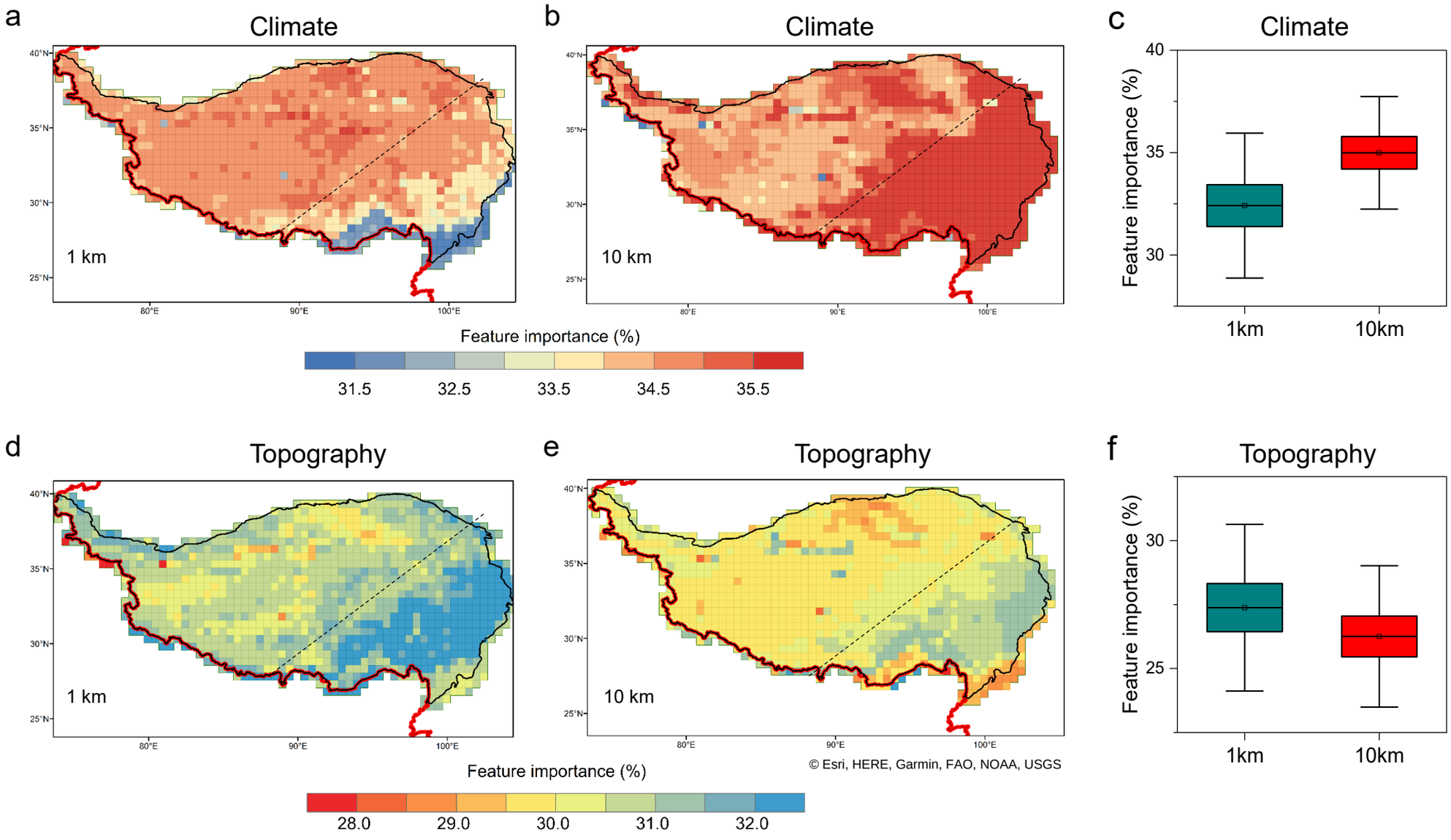
a
Climate
1 km
b
Climate
10 km
c
Climate
Feature importance (%)
40
35
30
1km
10km
Feature importance (%)
31.5
32.5
33.5
34.5
35.5
d
Topography
1 km
e
Topography
10 km
f
Topography
Feature importance (%)
30
25
1km
10km
© Esri, HERE, Garmin, FAO, NOAA, USGS
Feature importance (%)
28.0
29.0
30.0
31.0
32.0
40°N
35°N
30°N
25°N
80°E
90°E
100°E

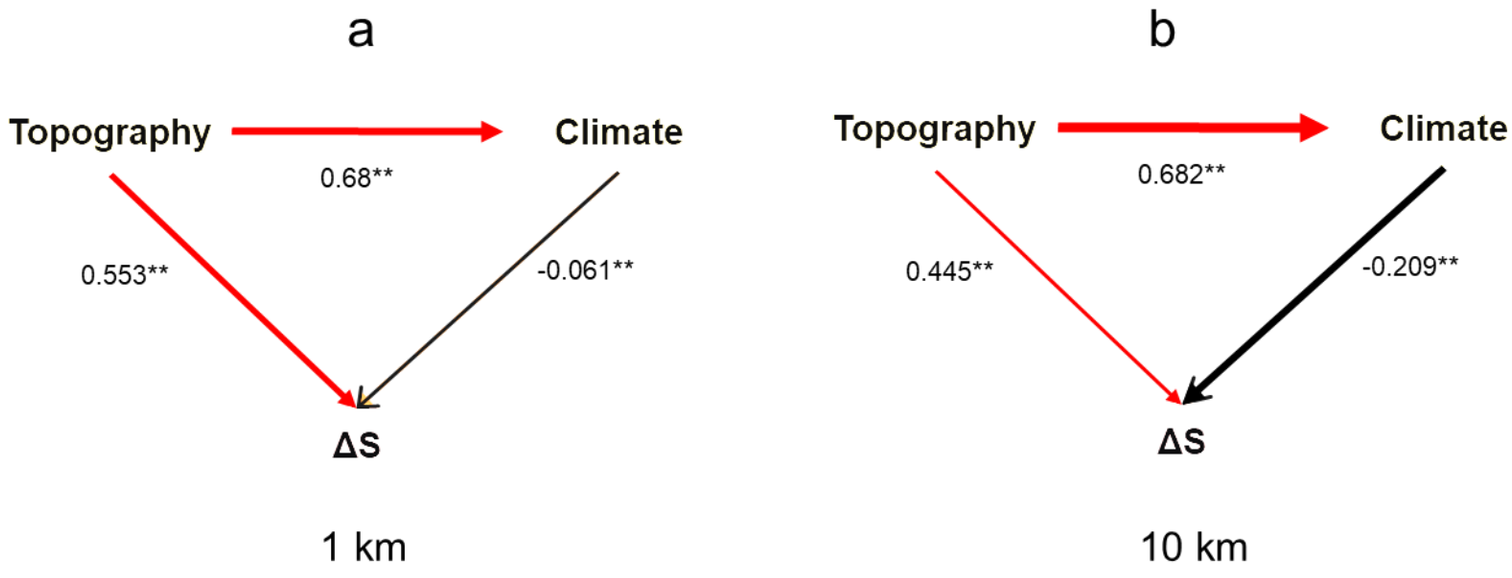
a
Topography
Climate
0.68**
0.553**
-0.061**
ΔS
1 km
b
Topography
Climate
0.682**
0.445**
-0.209**
ΔS
10 km